EasyChair Preprint

№ 9972

Dosimetric Study of Momentum Analysis System in a High Energy Proton Therapy System

Abdelkrim Zeghari, Rajaa Cherkaoui El Moursli and Rahal Saaidi

April 17, 2023

Dosimetric Study of Momentum Analysis System in a High Energy Proton Therapy System

A. ZEGHARI*[(1)], R. CHERKAOUI EL MOURSLI [(1)], R. SAADI[(2)]

[1] Laboratory of Nuclear Physics (ESMAR), Faculty of Sciences, Mohammed V University, Rabat, Morocco

[2] Institute of Applied Physics, Mohammed VI Polytechnic University, Lot 660, Hay Moulay Rachid, Ben Guerir, 43150, Morocco

a.zeghari@um5s.net.ma

Abstract. Recently, many worldwide leader societies try to develop its proton therapy technology. It strives to make proton therapy available to all cancer patients who could benefit from it to improve their quality of life. This is a shared purpose with radiation oncologists, medical physicists, radiotherapists and hospital directors around the world.

The introduction of proton therapy systems with the adjustments of the momentum analysis system, might have clinical consequences. The momentum analysis system normally alters the energy of the clinical proton beam, and hence the shape and position of the Bragg peak. FLUKA, a Monte Carlo based software was used to simulate different beam setups by dropping the proton beam in a water phantom. The Bragg peak were read out and compared to the Bragg peak with different setup simulations. The results have shown that the Bragg peak is changed for a proton therapy system with and without a modulator for all the possible tumors depth. The results obtained showed that the position of Bragg peak can changed from z = 31.4 cm for deep tumors as prostate to z = 2.6 cm for spinal axis tumors by just changing the depth of modulator from $\Delta Z_{modulator,\ PMMA} = 5$ to $\Delta Z_{modulator,PMMA} = 30$ cm for energy 250 MeV. It is recommended that this potential dosimetric consequence is investigated further for clinics who is interesting in obtaining such an proton therapy system.

Keywords: Proton therapy, FLUKA, Dose Distribution, Bragg-Peak, Modulator.

1 Introduction

Cancer is now considered as one of the major diseases affecting people in the developing countries more than 55 percent of new cases arise and 70 percent by 2050 according to a Havard study. According to the International Agency for Research on Cancer (IARC) and the World Health Organization (WHO), cancer could further increase by 50% to more than 15 million new cases in the year 2022. Cancer can develop in almost every kind of tissue at the skin or deep within the

body. The treatment field have need then to be adapted treat every possible kind of cancer, at any depth. A dose check is recommended before any treatment. The treatment plan defined all the beam parameters to be applied for patient to completely destroy cancerous cells. Therefore, the clinical application of such techniques requires a reliable estimate of the absorbed dose distributions to ensure the compromise of the need to sufficiently irradiate cancerous tissue and avoid to irradiate neighbouring healthy tissues. On that occasion, patient dosimetry then becomes the stage where treatment planning can be evaluated, experimentally verified, and finally validated. Monte Carlo (MC) methods are increasingly utilized for clinical treatment planning for these situations.

In 1927 the Norwegian physicist Rolf Widerøe developed the linear accelerator (linac). Linacs are used for accelerating electrons for electron and photon therapy, but linacs for protons would be too long to use in a clinical setting. Fortunately it is possible to gain higher kinetic energy by using circular accelerators. The cyclotron was invented in 1930 by E.O. Lawrence. It consists of two dipole magnets with a constant magnetic field B over a wide area. Charged particles placed in the middle of the cyclotron, where they are accelerated in a cavity with electrical potential.

In 1946 Robert R. Wilson proposed to use fast protons in cancer therapy. He had worked on cyclotrons. He argumented for that the Bragg curve made an ideal depth dose curve for the treating tumours and minimize the damage to healthy tissue. Robert R. Wilson hence marked the start of proton therapy and is today seen at the ”father of proton therapy” [1]. During the three next decades many research centres around the world starting treating patients as a part of their particles, including Russia, Japan and Switzerland. After 35 years of treating patients in research centres, the first full scale clinical centre was opened at Loma Linda Hospital (1990). It had is own designated synchrotron, made by physicists of Fermilab. Multiple treatment rooms for one single accelerator, became the standard for most of the new centres, optimizing the cost per patient. Recently, interest in radiation therapy with heavy ions such as protons has gained momentum, more than 200,000 patients were treated with protons in 110 centers around the world. The reason why proton therapy is preferred clinically is that higher doses can be given to the tumor compared to photon radiotherapy and better protection of healthy tissue [2].

Particle physics collaborations, for example at CERN (l'Organisation européenne pour la recherche nucléaire), have brought together part of thousands of scientists from every laboratories of the world to work on the largest and most complex experiments. Proton therapy could still be profitable, due to the reduction of secondary tumours. While proton therapy could be very effective for children, e.g. with brain melanoma, the gain to cost ratio is still low for seniors, e.g. prostate cancer [3-4]. The cost effectiveness would be one of the major focus areas of the community in the coming years. Proton therapy still have to prove that it is worth the money spent. As a response to the high investment cost, the most centers was based upon multiple treatment rooms and one accelerator, different companies today is delivering single room centers. Two companies, IBA and Mevion, have

installed the first centers are started treating patients. There are many approaches to the cost reduction, like building smaller accelerators, or smaller gantries [5].

The depth of the most distal edge of different tumour categories and the values have been read out, and fitted together with the Norwegian overview of possible patients. The spinal axis is skin close, the distal part of the planning treatment volume (PTV) is at most 6-7 cm from the surface of the back. But for prostate, the distal edge could between 23 cm and 32 cm from the surface of the body. These 32 cm is the reason why the accelerators need to be able to accelerate the protons all the way to 250 MeV or more. An 230-250 MeV is the standard extraction energy of clinical cyclotrons today, it would still be possible to treat many patients by using smaller accelerators. As an example, 50 % of the patients could still be treated with an maximum range of 17 cm [6].

Some companies, chose an ingenious solution for their center, by mounting the cyclotron on the gantry, they where able to fit the all equipment into a single room. And they kept the opportunity to treat from all angles and at all depths within the body. But by implementing the cyclotron onto the gantry, there was no room for a momentum analyser in the beam line. According to J.M. Schippers and A.J. Lomax, the difference in energy spread would enlarge the distal dose falloff of the Spread Out Bragg Peak (SOBP), which again would yield an extra unnecessary dose to other organs nearby [7-8-9]. The extra organ dose is difficult to measure, and changes from patient to patient. The distal dose falloff of a pristine Bragg peak is a generic and physical distance, independent of which supplier of the momentum analyzer free system. The parameter was quantified for different treatment depths within the body by simulating a proton beam with an MC techniques. By quantifying the distal dose falloff as a function of treatment depths, it is be possible to compare the system with a momentum analyzer to the systems without a momentum analyzer.

In this study, the Bragg curves of protons from 50 MeV to 250 MeV by a step of ΔE=20 MeV were investigated inside a water phantom were obtained using the FLUKA MC simulation software. The Bragg curve dose of proton beams in the water phantom were calculated and compared with each other.

2 Materials and Methods

2.1 Synchrotron/ESS Monte Carlo Simulation

The FLUKA code CERN version V4-2.2 was used together with a graphical user interface software, Flair v.2.0-3 for dose calculations. A simple model was made, as seen in figure 1.

The model was based around a small water phantom. The proton beam was dropped was i every experiment initialized i x=0, y=0, z=-150cm and sent directly towards the water phantom. To make the experiment as realistic as possible, all of the parameters used was gather from other research papers. The experiment was done by comparing some different main setups, which focused on the different pa-

rameters from different papers. The setups were categorized into two categories: “The Synchrotron/ESS setups“, and the ”Modulator setups“, where the latter lacks the MAS.

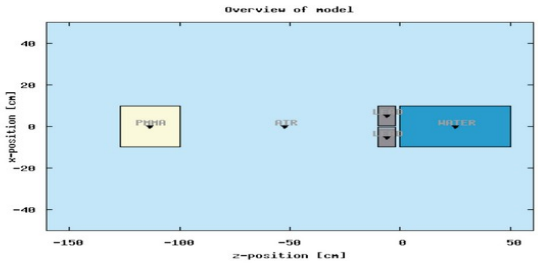

Fig. 1. A XZ view at y=0 of the FLUKA model used in the Monte Carlo Simulation.

The beam was initialized in z= -150 cm with a variable energy E. The value is taken from the patent of synchrotron at the Heidelberger Ionenstrahl Therapiezentrum (HIT), a modern particle therapy synchrotron [10].

A system with a full energy selection system (ESS) is able to adjust the energy spread σ_E by adjusting the width of the momentum colimator [11]. A depth dose curve would be technical achievable by placing a colimator made by a high Z material in the beam between the source and the patient [12]. The parameters, $\sigma_x = \sigma_y$ = 4.25 mm used for the synchrotron setup, was taken from a research paper by K. Parodi and W. Enghardt [13].

12 runs was simulated of the two synchrotron/ESS setups with different energies, at steps of ΔE = 20 MeV from E= 50 MeV to E = 250 MeV without the modulator. Then a 6 runs was simulated of the different modulator materials. After that, we simulated a total of 17 runs of the modulator thickness, in step of $\Delta z_{modulator}$ = 5 cm: from $\Delta z_{modulator}$= 0 cm to $\Delta z_{modulator}$ = 25 cm for energies 230 MeV, then from $\Delta z_{modulator}$ = 5 cm to $\Delta z_{modulator}$ = 30 cm for energies 250 MeV and finally from $\Delta z_{modulator}$= 10 cm to $\Delta z_{modulator}$ = 30 cm for energies 270 MeV. Also, we run 5 simulations for different materials colimator. Every run tracked 1×10^6 initial protons each, which gave an ”acceptable“ error for most runs. The dose ($Gy \times cm^2/10^6$ protons) was detected in the water phantom along the axis by a cylindrical detector.

The result was then plotted with gnueplot program to exemplify the different depth dose for the full Bragg-peaks curves for all setups. Also a lateral map of the x-axis was detected to show the lateral spread. All the simulations were run on a desktop core i7 CPU with 16 GHz RAM on Ubuntu 20.04.5 system using the FLUKA/FLAIR code.

2.2 Modulator and Momentum Analysis System

In recent active scanning nozzles have no components in the trajectory of the beam, a simple synchrotron/ESS setup is easy to model. But a compact proton therapy system would be a bit more complex, since all beam components need to be placed in the nozzle, between the accelerator and the patient. The Mevion S250 was only one kind of compact therapy system without a momentum analysis sys-

tem (MAS). Since we are interesting in looking at the Bragg-Peak dependency, we could further simplify the model to only include the modulator.

Cyclotrons are only able to extract their beam at the maximum treatment energy, so the beam has to be modulated to achieve lower energies. The modulator is most certainly made of a material with low Z, which relatively stops the beam more than it scatters, compared to high Z material. In our model, the modulator is then set to Poly Methyl Meth Acrylate (PMMA), a typical material in a modulator. In the synchrotron/ESS setups, the initial energy E is varied to change the range, while in the modulator setup, the thickness of the modulator is varied. The beam can be adjusted so that the Bragg peak is placed at the tumor site. The proton energy is changed by passing the beam through a modulator and many Bragg peaks occur at various depths. The modulator (degrader) is able to change the energy by adjusting the thickness of the material which the beam has to pass through the different tumor depth categories as indicated the Fig 2. The energy adjustment should be done as fast as possible to get rid of interpolation effects, one of the greatest issues in modern proton therapy [12].

To mimic a realistic beam of a system without a MAS, the initial beam parameters is taken from research papers about the Mevion system, the beam is initialized with an energy E = 250 MeV in positive z-direction at z = -150 cm. In a research paper the energy spread from the synchrocyclotron is σ_E = 0.42 MeV [14].

The protons also scatterings a lot in the modulator, which will widen the focus of the beam at the phantom water entrance. This could be done by a small passive colimator of lead with a circular hole. In a paper about the passive scattering system in Mevion, a passive high Z colimator is placed 2 cm in front of the water phantom [9]. The thickness is set to a constant of 8 cm to be assure there will be no radiation behind, even though such a metal is far to heavy for clinical use.

In the conference proceeding by Bloch et. al., the σ_E value from the accelerator was chosen to 1.4 MeV, based upon fitting of σ_E to measurements on the first Mevion S250 in clinical use.

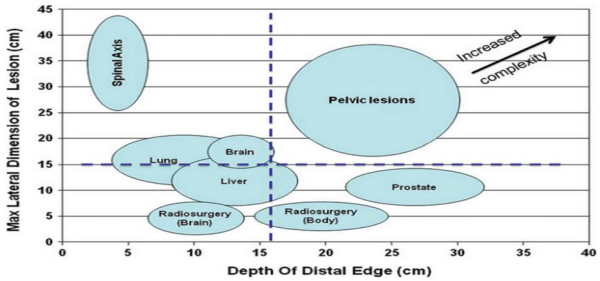

Fig. 2. An illustration over the maximum lateral and distal limits of the treatment fields of different cancer categories. [15]

2.3 Bragg curve and Range Straggling

The Bragg curve, which is the relative depth dose curve, gets its characteristic shape from three main interactions which occur between the accelerated protons and matter.

The shape of the ionization curve is strongly dependent on the energy of the protons. Range straggling, a phenomenon which the protons travel into matter before they come to a halt. The mean range R can be calculated using the "continuous slowing down approximation", by integrating over the stopping power for energy from E to 0:

$$R(E) = \alpha E^{p} \quad \textbf{(1)}$$

International Commission on Radiation Units & Measurements (ICRU) have experimentally given $\alpha \approx 2.2\times10^{-3}$ cm.MeV and $p \approx 1.77$ for protons passing through water [16].

Since all of the particles interactions (stopping, scattering and nuclear interactions) are randomized processes, the particles in a beam will not have the same number of collisions. So every proton would not have the same range in the material, even for monoenergic protons in a homogeneous material [17].

3 Results and Discussions

The presented FLUKA-based tool is able to calculate the depth dose ($Gy\times cm^2/10^6$ protons) curve for all kinds of geometrical configurations and incident beams. For the incident beams considered in this work, the increase of energy towards the water phantom increase the position of Bragg peaks. It is clear from the present study that the contribution of the proton particles due to principal interactions influences the distribution of the position of Bragg peaks-dose. For the incident proton beams, some investigations have been done in order to understand how to take into account these contributions for biological assessments. In these studies, MC approach were used to take into account the proton dose distributions in water phantoms.

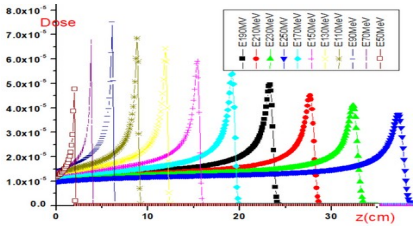

Fig. 3. Absorbed dose as a function of depth z in a water phantom for Bragg peaks produced by a proton beams with an initial energies from 50 MeV to 250 MeV.

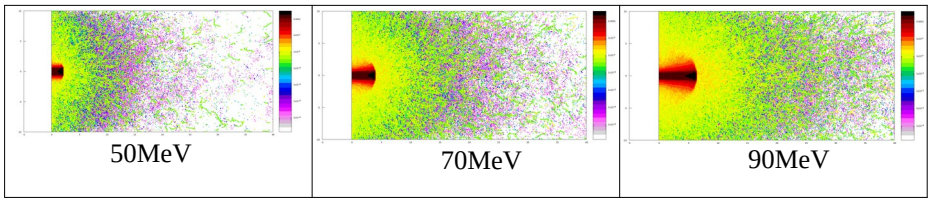

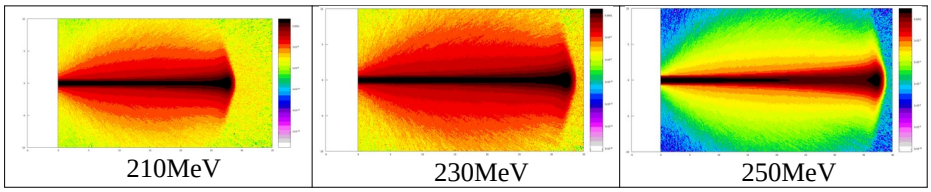

Fig. 4. Energy deposition (x,z) profile of energies for some beams proton energies inside the water phantom simulated using FLUKA-USRBIN.

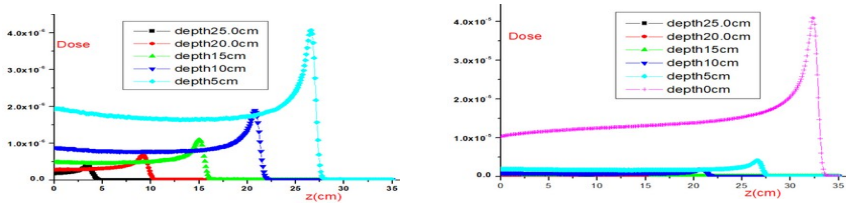

Fig. 5. Depth dose distributions of 230 MeV proton beams inside a water phantom with depth modulator from ΔZ_{modul}=0 to ΔZ_{modul}=25 cm.

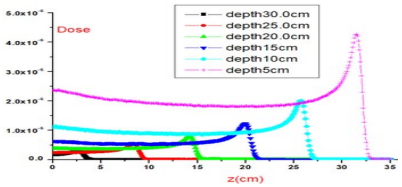

Fig. 6. Depth dose distributions for 250 MeV proton beams inside a water phantom with depth modulator from ΔZ_{modul}=5 cm to ΔZ_{modul}=30 cm.

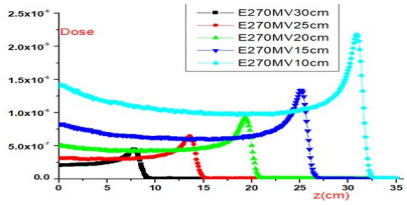

Fig. 7. Depth dose distributions of 270 MeV proton beams inside a water phantom with depth modulator from ΔZ_{modul}=10 cm to ΔZ_{modul}=30 cm.

Figure 3 showed a comparison of different FLUKA calculated depth dose of Bragg-peaks on a water phantom for some energies values varied from 50 MeV to 250 MeV beams. Figure 4 exposed the absorbed dose distribution (x,z) profile along the z axis for the energies varied from 50 MeV to 250 MeV beams on a water phantom. Figure 5 illustrated the variation of depth dose distributions of 230 MeV proton beams inside a water phantom with a modulator thickness altered from ΔZ_{modul}= 0 to ΔZ_{modul}= 25 cm. Figure 6 presented the depth dose distributions of 250 MeV proton beams inside a water phantom with a modulator thickness changed from ΔZ_{modul}=5 cm to ΔZ_{modul}=30 cm. Figure 7 illustrated the variation of

depth dose distributions of 270 MeV proton beams inside a water phantom with a modulator thickness varied from ΔZ_{modul} = 10 to ΔZ_{modul}= 30 cm. Figure 8 presented the depth dose distributions of 250 MeV proton beams inside a water phantom when we changed the materials of modulator as (PMMA, Polyethylene, Polystyrene, Plastic scintilator). Figure 9 presented the depth dose distributions of 250 MeV proton beams inside a water phantom with different materials colimator.

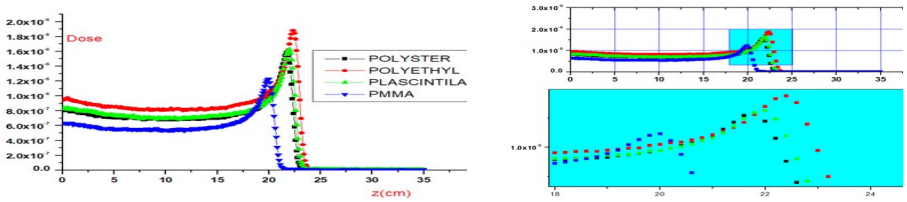

Fig. 8. Depth dose distributions of 250 MeV proton beams inside a water phantom for different modulator materials (PMMA, Polyethylene, Polystyrene, Plastic scintilator).

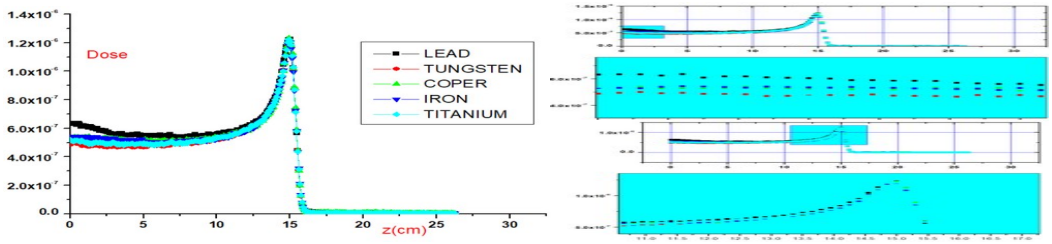

Fig. 9. Depth dose distributions of 250 MeV proton beams inside a water phantom with varied colimator materials.

Table 1. MC calculated ranges for 50, 150 and 230 MeV primary proton energies in the water phantom.

Energy(MeV)	FLUKA(cm)	GATE/Geant4(cm)[18]	MCNP6(cm)[18]
50	2.2	2.22	2.22
150	15.4	15.73	15.69
230	32.3	32.86	32.74

As a starting point of the discussion, in this section we will discuss the influence of physical and radio biological properties of proton beams which provide a superior dose distribution compared to photon radiotherapy, thus minimizing the dose delivered to normal tissues [19]. Thus, the risk of secondary cancer is significantly reduced, by investigating the variation of modulator thickness and materials on the position of the Bragg peak. Figure 3 shows different initial energies of proton beams without modulator which have changed the position of the Bragg peak from z=37.3 cm for 250 MeV to z=1.8 cm for energy 50 MeV that create a continuous spectrum of the absorbed dose in the diverse tumor region to be treated. Figure 4 shows the energy deposition (x,z) profile of energies from 50 MeV to 250 MeV protons inside the water phantom simulated using FLUKA-USRBIN. Figure 5

shows different thicknesses of PMMA from $\Delta Z_{modul,PMMA}$=0 to $\Delta Z_{modul,PMMA}$=25 cm for 230 MeV to create a continuous spectrum of the absorbed dose in the tumor region based on the Bragg peak position. So the effect of modulator PMMA material thicknesses was important in this study as this registered a diminution of the Bragg peak position from z =32.3 for $\Delta Z_{modul,PMMA}$=0 cm to z=3.5 cm for $\Delta Z_{modul,PMMA}$=25 cm. Figure 6 shows the influence of different thicknesses of PMMA from $\Delta Z_{modul,PMMA}$=5 to $\Delta Z_{modul,PMMA}$=30 cm for 250 MeV to create a continuous spectrum of the absorbed dose in the tumor region based on the Bragg peak position. So the effect of modulator PMMA material thicknesses was important in this study as this registered a diminution of the Bragg peak position from z=31.4 for $\Delta Z_{modul,PMMA}$=5 cm to z =2.6 cm for $\Delta Z_{modul,PMMA}$ =30 cm. Figure 7 shows the influence of different thicknesses of PMMA from z=10 to z=30 cm for 270 MeV to create a continuous spectrum of the absorbed dose in the tumor region based on the Bragg peak position. So the effect of modulator PMMA material thicknesses was important in this energy as this registered a diminution of the Bragg peak position from z=30.9 for $\Delta Z_{modul,PMMA}$=10 cm to z =2.6 cm for $\Delta Z_{modul,PMMA}$=30 cm. Figure 8 shows the variation of the Bragg peak position with different modulator materials. So the effect of modulator material was important in this study as this registered a small increase in the Bragg peaks position when we substituted the PMMA by Polyethylene material from z=20 to z=22.3 cm [20]. Figure 9 illustrated the variation of the Bragg peak position with different colimator materials. So the effect of colimator material was not important on the Bragg peaks position when we substituted the Lead material by others material. But, we observed a small decrease on the entrance dose by a factor of 1.3 when we replaced the Lead colimator by Tungsten colimator.

The simulation results show that when the proton beam has energy of 230 MeV without degrader and 250 MeV with $\Delta Z_{modul,PMMA}$=5 cm and 270 MeV with $\Delta Z_{modul,PMMA}$=10 cm, the Bragg peak was formed at the end of the tumor region. Research has been done to use low Z materials, such as PMMA, to change the range of protons and high Z materials, such as Lead, to create lateral scattering.

From the simulation of the 250 MeV proton beam with different thicknesses of a modulator, several Bragg peaks are created in the tumor region. With increasing the thickness of the modulator, the created Bragg peaks cover the entire tumor volume.

4 Conclusions

A FLUKA MC model was successfully constructed for a range 50 - 250 MeV proton beams incident as MAS accelerators on a cubic water phantom. This paper investigates the modulator thicknesses and materials and colimator materials on Bragg curves calculated with FLUKA/FLAIR MC code. The principal results of this paper is to establish that, when various thicknesses of a modulator simulated, several Bragg peaks are created to cover the entire tumor volume. So the findings revealed that the Bragg peak position can take different positions with the same energy when we varied the modulator thickness to treat many categories of tumors without changing the incident proton beams energy.

Finally, the paper are useful on improving the usability of the proton therapy tool and extending the range of applications for clinical and research environment.

References

1. R.R. Wilson, Radiological use of fast protons. Radiology 47.5 487-491 (1946).
2. Dowdell, S. J., Pencil beam scanning proton therapy: the significance of secondary particles, University of Wollongong, Australia, (2011).
3. A. Konski, et. al, Is proton beam therapy cost effective in the treatment of adenocarcinoma of the prostate?. Journal of Clinical Oncology 25.24 3603-3608 (2007).
4. T. Björk-Eriksson and B. Glimelius, The potential of proton beam therapy in paediatric cancer. Acta Oncologica 44.8 871-875 (2005).
5. K.P. Gall, The Single-Room Ion Beam Facility Ion Beam Therapy: Fundamentals, Technology, Clinical Applications, Springer 661-717 (2012).
6. T. Haberer et al., Ion beam therapy system and a method for operating the system. Google Patents, (2004).
7. J.M. Schippers and A.J. Lomax, Emerging technologies in proton therapy. Acta Oncologica **50.6** 838-850 (2011).
8. C. Bloch et al., Startup of the Kling Center for Proton Therapy in AIP Conference Proceedings 1525 314-318 (2013).
9. P.M Hill et al., Optimizing field patching in passively scattered proton therapy with the use of beam current modulation Phys Med Biol. 58.16 5527-5539 (2013)
10. T. Haberer et al., Ion beam therapy system and a method for operating the system. Google Patents, (2004).
11. S.A. Kostromin, E.M. Syresin, Trends in accelerator technology for hadron therapy Phys. Part. Nuclei Lett. 10 833–853 (2013).
12. B. Gottschalk, Passive Beam Scattering Proton and Charged Particle Therapy Radiotherapy, Lippincott Williams & Wilkins 33-40 (2008).
13. K. Parodi and W. Enghardt, Potential application of PET in quality assurance of proton therapy. Phys. Med. Biol. 45.11 N151-6 (2000).
14. K. L. Chen et al., Evaluation of neutron dose equivalent from the Mevion S250 proton accelerator: measurements and calculations. Phys. Med. Biol. 58.24 8709 - 8723 (2013).
15. J. Cameron and N. Schreuder, Smaller – Lighter – Cheaper: New Technological Concepts in Proton Therapy Ion Beam Therapy: Fundamentals, Technology, Clinical Applications, Springer 673-686 (2012).
16. ICRU Report 49. (1993). International Commission on Radiation Units and Measurements: Stopping Powers and Ranges for Protons and Alpha Particles.
17. U. Linz, Physical and Biological Rationale for Using Ions in Therapy Ion Beam Therapy: Fundamentals, Technology, Clinical Applications, Springer 45-60 (2012).
18. J. R. Sølie , H. E. S. Pettersen, I. Meric, O. H. Odland, H. Helstrup, D. hrich, “A comparison of proton ranges in complex media using GATE/Geant4, MCNP6 and FLUKA.” arXiv: Medical Physics (2017): n. pag.
19. F. Ekinci, E. Bostanci, Ö. Dagli and M. S. Guzel, Analysis of Bragg curve parameters and lateral straggle for proton and carbon beams, Commun.Fac.Sci.Univ.Ank.Series Vol 63, N 1, pages 32-41 (2021).doi:10.33769/aupse.864475.
20. Hu M, Jiang L, Cui X, et al. Proton beam therapy for cancer in the era of precision medicine. J Hematol Oncol. ;11:136-157 (2018).http://dx.doi.org/10.1186/s13045-018-0683-4.